Quantum Electronics **50** (7) 679–682 (2020)

https://doi.org/10.1070/QEL17292

Features of correlation measurements of the parameters of pulsed hyperspectral optical fields using an asymmetric interferometer

M.S. Kulya, V.Ya. Katkovnik, K. Egiazarian, N.V. Petrov

Abstract. **Differences in correlation measurements of the parameters of pulsed hyperspectral optical fields using symmetric and asymmetric interferometers are considered. It is shown analytically that the resulting cross-correlation function is sensitive to phase perturbations in the original wave field. The considered setup, which contains a telescopic reflective 4*f* system of parabolic mirrors in one arm, demonstrates that in the case of an asymmetric interferometer, the presence of aberrations leads to degradation of the reconstructed image, whereas in the case of symmetric interferometers these aberrations do not affect the result.**

Keywords: *hyperspectral fields, correlation measurements, symmetric and asymmetric interferometers.*

Hyperspectral interferometry (HI), first demonstrated in work [1], is a powerful tool for determining the shape of a broadband wavefront and for measuring both the amplitude and phase characteristics of objects, including those with refractive index dispersion. A distinctive feature of HI is obtaining the spatial distribution of broadband wavefronts with high spectral resolution, which allows one to reconstruct information about the object topography or the spatial distribution of its refractive index as a function of the radiation frequency. To implement this into practice, a series of interferograms is recorded when one signal shifts in time relative to the other in one of the interferometer's arms. Thus, the recorded series of broadband radiation interferograms represents a correlation function [1], to which the Fourier spectroscopy formalism is applied, which gives information about the spectral power density.

Modern HI methods can be systemised depending on the type of the radiation source used. The first type includes broadband sources with low temporal and high spatial coherence [2, 3]. These are heat sources [1] and light-emitting diodes [4], the individual radiation spectral components of which do not have to be strictly phase-matched, as in the case of the second type sources that generate ultrashort laser pulses by locking the laser resonator modes. HI with low-coherent radiation sources is commonly used to study objects placed in one of the arms of an asymmetric interferometer [5, 6]. It is also important to note that obtaining radiation with such coherent properties is usually associated with energy losses, which makes HI methods sensitive to noise. In addition, when propagating through an optical system, the spectral composition of radiation may change due to inhomogeneous spectral absorption, chromatic aberrations resulting from the presence of optical elements with refractive index dispersion, and other wavefront distortions. It is assumed that the noise arising in the system can be described by a model of identically distributed additive noise with a Gaussian distribution of its standard deviation [7]. A significant improvement in this HI type was due to the use of more advanced noise suppression algorithms based on the use of sparse representations of hyperspectral images [7, 8].

Another class of HI methods is used to characterise ultrashort laser pulses [9, 10]. Here, interference patterns are also sequentially recorded depending on the time delay between the signals, but now a pair of pulses acts as signals, and both asymmetric [9] and symmetric [10] interferometers are used. Due to a physical generation mechanism that uses mode locking to form ultrashort pulses, laser radiation can have a unique spatio-temporal distribution and spectral phase, which is also often associated with various spatiotemporal connectivity effects [11]. To solve modern scientific problems involving the use of ultrashort laser pulses, it is extremely important to have access to all the characteristics of a broadband complex-valued field.

Special attention should be paid to hyperspectral measurements implemented in the terahertz (THz) frequency range in the pulsed regime, in which solutions to both previously mentioned problems, namely characterisation of objects [12] and wavefront metrology [13–15], have already been demonstrated using a method known as terahertz pulse time-domain holography (THz PTDH). Despite the fact that interferometric recording, although in a slightly different form, is still possible here [16], in general, these methods already go beyond interferometry and relate to digital holography, since instead of recording the results of interference between the reference and object waves, electro-optical detection is implemented here [17]. It is based on recording the correlation function of a THz pulse with a reference femtosecond pulse of the near-infrared spectrum range, which allows us to consider the latter as a delta-function during measurements. Owing to these features, these methods provide direct access to the spectral phase, which implies that the phase spectral distribution can be directly calculated using the Fourier transform applied to the measured temporal dependence of the real

M.S. Kulya, N.V. Petrov ITMO University, Kronverkskii prosp. 49, 197101 St. Petersburg, e-mail: n.petrov@niuitmo.ru;
V.Ya. Katkovnik, K. Egiazarian Tampere University, Faculty of Information Technology and Communication, TampereFI-33014, Finland

Received 18 February 2020; revision received 15 April 2020
Kvantovaya Elektronika **50** (7) 679–682 (2020)
Translated by M.A. Monastyrskiy

part of the THz field amplitude. It should be noted separately that this feature is one of the major differences between the hyperspectral holographic methods of the THz frequency range and the HI methods used for measuring fields of pulsed femtosecond radiation [9, 10], in which the use of the Fourier transform does not provide access to the signal's spectral phase in one of the interferometer's arms, and additional iterative algorithms are then used to obtain it. Also, speaking about the differences in the THz-range techniques, it is worth mentioning work [18], in which imaging is implemented by measuring the cross-correlation function between two terahertz pulses, but not only by the interaction of optical and THz radiations.

The aim of this work is to consider and analyse the features of the correlation measurement of femtosecond broadband laser fields using the HI methods. While in the HI methods employing continuous-wave broadband sources, obtaining the phase characteristics of radiation passed through the object under study assumes the presence of a perfectly collimated plane wavefront in both arms, the existence of a consistent spectral phase for individual frequency components introduces additional specificity in the case of ultrashort pulse sources. Therefore, a more complicated case, when the wavefront contains a spatial-phase structure different from the structure of a plane wave requires a separate study.

Figure 1 shows a scheme of the HI setup used in this work. It is based on an asymmetric Mach–Zehnder interferometer with a delay line (DL) in the reference arm. A beam in the object arm, formed by a pellicle beam splitter (BS), passes through the object, and its image is formed on the matrix photodetector (CMOS) using a telescopic reflex 4*f* system that has a unit magnification factor and consists of two parabolic mirrors (PM). Note that off-axis parabolic mirrors in the 4*f*-system design are commonly used in setups operating with ultrashort pulses, which are extremely sensitive to the effects of refractive index dispersion that manifest themselves during the propagation of such pulses through optically transparent materials. The reference and object waves overlap in the recording plane. As will be clear from what follows, an important aspect of this work is the absence of a telescopic 4*f* system in the reference arm, similar to that used in the object arm, which makes the reference wave susceptible to diffraction. Thus, if there is a perturbation in both interferometer arms, diffraction provides a phase shift at each spatial point of the cross-correlation function, which leads to distortion of the reconstructed image.

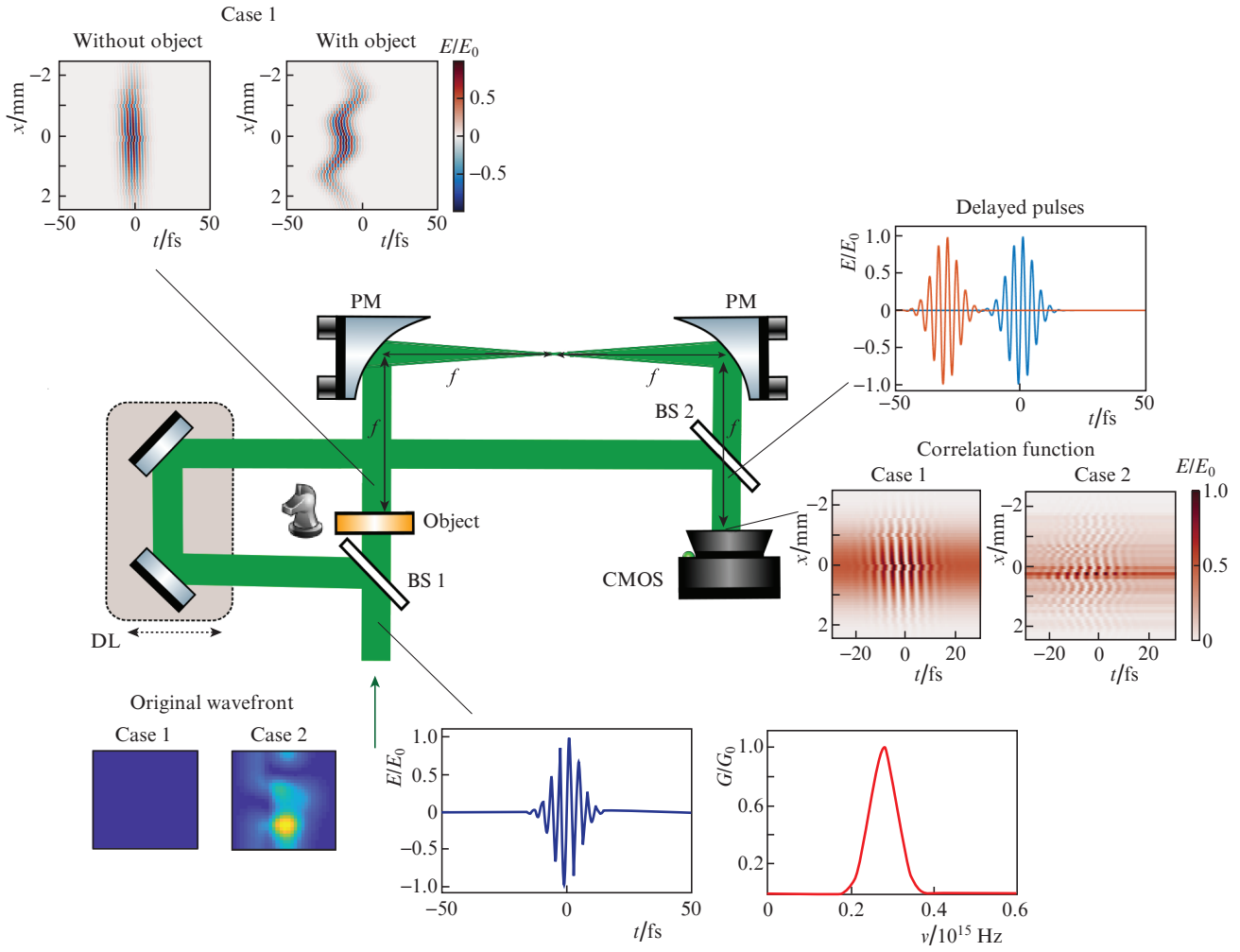

Figure 1. Schematic of the setup for correlation measurements of the parameters of pulsed hyperspectral optical fields using digital holography methods:
(BS) beam splitter; (DL) motorised delay line; (PM) parabolic mirror; (CMOS) detector. The insets show the characteristics of simulated pulses.

In this work, we consider the solution of direct and inverse problems, which consist in simulating the process of forming cross-correlation signals at the detector and extracting the amplitude–phase characteristics from them. Two different cases are considered (Fig. 1): case 1 corresponds to a plane wavefront at the setup input, and case 2 assumes the presence of phase distortions of the wavefront.

Insets in Fig. 1 show the characteristics of the simulated pulses. The following parameters were used in the simulation: the initial pulse duration was $\tau = 10$ fs, the reference pulse displacements relative to the object pulse were in the range $-30 \div 30$ fs. These phase distortions of the input pulse were set by using a phase mask with a spatial distribution corresponding to the standard 'peaks' function in MATLAB. It was assumed that the maximum height difference in the mask was $15\lambda_0$, where $\lambda_0 = 800$ nm, and the refractive index was 1.4. Figure 1 also shows the original femtosecond pulse and its temporal spectrum.

Consider a mathematical model for this type of HI. The final cross-correlation function recorded on the detector can be written as follows:

$$I(x,y,\tau) = \int_0^\infty |AS_\nu[O(x,y,\nu)b(x,y,\nu)] + AS_\nu[R(x,y,\nu)b(x,y,\nu)]\exp(-\mathrm{i}2\pi\nu\tau)|^2 \mathrm{d}\nu, \quad (1)$$

where $O(x,y,\nu)$ is the spatial-frequency function of the object's field; $R(x,y,\nu)$ is the reference field function; $b(x,y,\nu)$ is the accumulated wavefront perturbation in the BS_1 plane (we consider the approximation in which the object is located infinitely close to BS_1); the reference beam's phase shift is determined by the parameter τ. Here, we first describe the general case when the reference and object wavefronts can undergo diffraction, which can be taken into account using the AS_ν wavefront propagation operator for time frequencies, as was done in our previous work [10–13]. In this case, we only consider positive frequencies $\nu > 0$ that have a physical meaning. Then this cross-correlation function can be represented in the form:

$$\begin{aligned} I(x,y,\tau) = \int_0^\infty \mathrm{d}\nu \{ & |AS_\nu[O(x,y,\nu)b(x,y,\nu)]|^2 \\ & + |AS_\nu[R(x,y,\nu)b(x,y,\nu)]\exp(-\mathrm{i}2\pi\nu\tau)|^2 \\ & + AS_\nu[O(x,y,\nu)b(x,y,\nu)] \\ & \times \{AS_\nu[R(x,y,\nu)b(x,y,\nu)]\}^* \exp(\mathrm{i}2\pi\nu\tau) \\ & + \{AS_\nu[O(x,y,\nu)b(x,y,\nu)]\}^* \\ & \times AS_\nu[R(x,y,\nu)b(x,y,\nu)]\exp(-\mathrm{i}2\pi\nu\tau)\}. \end{aligned} \quad (2)$$

Here "*" is the complex conjugation. The subsequent Fourier transform in q frequencies for the cross-correlation function yeilds the expression

$$\begin{aligned} I(x,y,q) &= \int_{-\infty}^\infty I(x,y,\tau)\exp(-\mathrm{i}2\pi q\tau)\mathrm{d}\tau \\ &= \int_{-\infty}^\infty \exp(-\mathrm{i}2\pi q\tau)\mathrm{d}\tau \int_0^\infty |AS_\nu[O(x,y,\nu)b(x,y,\nu)]|^2 \mathrm{d}\nu \\ &+ \int_{-\infty}^\infty \exp(-\mathrm{i}2\pi q\tau)\mathrm{d}\tau \int_0^\infty |AS_\nu[R(x,y,\nu)b(x,y,\nu)]|^2 \mathrm{d}\nu \\ &+ \int_{-\infty}^\infty \exp[-\mathrm{i}2\pi(q-\nu)\tau]\mathrm{d}\tau \int_0^\infty AS_\nu[O(x,y,\nu)b(x,y,\nu)] \\ &\times \{AS_\nu[R(x,y,\nu)b(x,y,\nu)]\}^* \mathrm{d}\nu \\ &+ \int_{-\infty}^\infty \exp[-\mathrm{i}2\pi(q+\nu)\tau]\mathrm{d}\tau \int_0^\infty \{AS_\nu[O(x,y,\nu)b(x,y,\nu)]\}^* \\ &\times AS_\nu[R(x,y,\nu)b(x,y,\nu)]\mathrm{d}\nu, \end{aligned} \quad (3)$$

and integration by τ yields

$$\int_{-\infty}^\infty \exp(-\mathrm{i}2\pi q\tau)\mathrm{d}\tau = \delta(q),$$

where $\delta(q)$ is the Dirac delta function. Accordingly, Eqn (3) takes the form:

$$\begin{aligned} I(x,y,q) &= \int_0^\infty |AS_\nu[O(x,y,\nu)b(x,y,\nu)]|^2 \delta(q)\mathrm{d}\nu \\ &+ \int_0^\infty |AS_\nu[R(x,y,\nu)b(x,y,\nu)]|^2 \delta(q)\mathrm{d}\nu \\ &+ \int_0^\infty AS_\nu[O(x,y,\nu)b(x,y,\nu)] \\ &\times \{AS_\nu[R(x,y,\nu)b(x,y,\nu)]\}^* \delta(q-\nu)\mathrm{d}\nu \\ &+ \int_0^\infty \{AS_\nu[O(x,y,\nu)b(x,y,\nu)]\}^* \\ &\times AS_\nu[R(x,y,\nu)b(x,y,\nu)]\delta(q+\nu)\mathrm{d}\nu. \end{aligned} \quad (4)$$

Thus, for solutions having physical meaning at frequencies $\nu > 0$ and $q > 0$, we obtain:

$$I(x,y,q) = AS_q[O(x,y,q)b(x,y,q)] \times \{AS_q[R(x,y,q)b(x,y,q)]\}^*. \quad (5)$$

Equation (5) describes the resulting cross-correlation function in the frequency domain q. An important consequence of this is that if the wavefront propagation operator AS_q acts equally in the reference and object arms, then the perturbation $b(x,y,q)$ does not contribute to the cross-correlation function's phase by virtue of the product $b(x,y,q) \times b(x,y,q)^*$. Herewith, if the object arm contains a 4f system with a unit magnification coefficient (as shown in Fig. 1), the resulting equation for $I(x,y,q)$ does not contain the AS_q operator in the first multiplier. Therefore, this result will depend on the perturbation $\{AS_q[b(x,y,q)]\}^*$ in the second multiplier. Thus, if $b(x,y,q)$ in the reference beam is a plane wave (the perturbation is absent, case 1 in Fig. 1), then $\{AS_q[b(x,y,q)]\}^* = b(x,y,q)^*$, and the contribution of this perturbation to the phase will also be compensated for by the product $b(x,y,q) \times b(x,y,q)^*$. However, if $b(x,y,q)$ describes a structure different from the structure of a plane wave (case 2 in Fig. 1), we obtain $b(x,y,q)\{AS_q[b(x,y,q)]\}^*$, and the perturbation phase $b(x,y,q)$ will affect the result of image reconstruction.

Figure 2 shows the result of solving the inverse problem, and the reconstructed phase distributions of the wave field for cases 1 and 2 are given for different frequencies. It can be seen

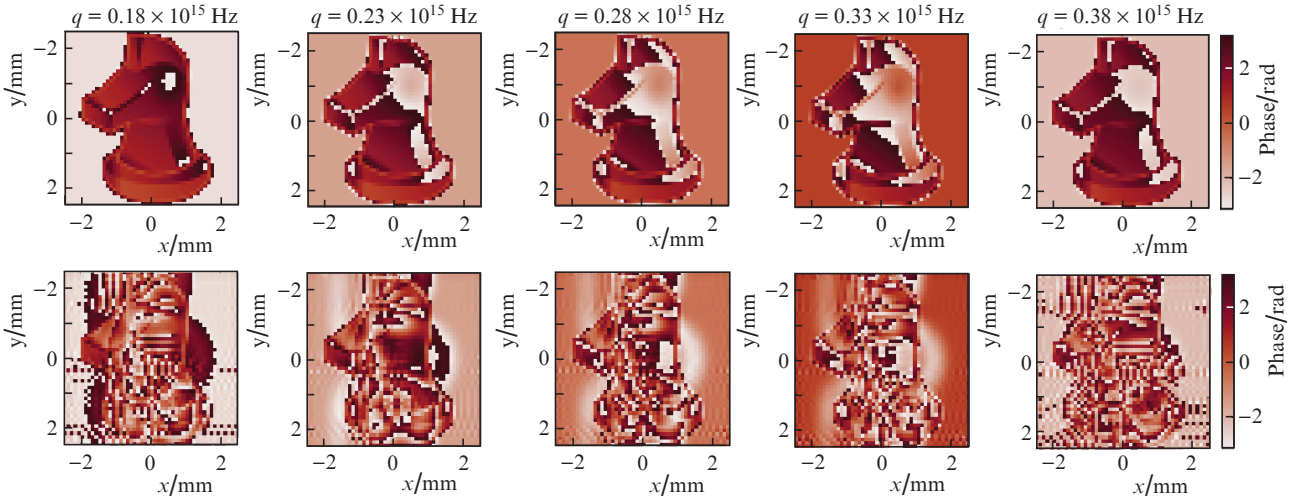

Figure 2. Spatial-phase structures of the cross-correlation function $I(x, y, q)$ for several frequencies q. Case 1 (upper row) displays a plane wavefront; case 2 (bottom row) shows a wavefront with accumulated phase perturbations.

that in the case of a plane wavefront in both arms of an asymmetric interferometer, the cross-correlation function's phase correctly displays the object. If the original wavefront has phase inhomogeneities, the reconstructed spatial-phase characteristics of the radiation will be distorted by fluctuations both at the edges and at the centre of the image, which will not allow correct determination of the object profile.

Thus, in this work, we have considered the features of correlation measurements of parameters of pulsed hyperspectral optical fields in an asymmetric interferometer. Based on the analytical equation (5), the impact of diffraction on the spatial-phase structure of the reference and object waves has been analysed and the HI model limitedness to the case of using a plane wavefront at the asymmetric interferometer input is justified. Thus, it is shown that in the scheme using a 4*f* system in the object beam, the resulting cross-correlation function depends on the degree of phase perturbation in the original wave field. A significant difference is observed in the quality of phase image reconstruction of an object with an originally plane wavefront and a wavefront having certain accumulated phase perturbation. Therefore, in general case, the complete reconstruction of the phase characteristics of a pulsed wavefront requires algorithms that allow spectral matching of the pulse's individual frequency components [9, 10].

Acknowledgements. This work was supported by the Russian Foundation for Basic Research (Grant No. 18-32-20215).

References

1. Itoh K. et al. *Appl. Opt*., **29** (11), 1625 (1990).
2. Naik D.N., Pedrini G., Takeda M., Osten W. *Opt. Lett*., **39**, 1857 (2014).
3. Kalenkov S.G., Kalenkov G.S., Shtanko A.E. *J. Opt. Soc. Am. B,* **34**, B49 (2017).
4. Claus D., Pedrini G., Buchta D., Osten W. *Proc. SPIE,* **10335**, 103351H (2017).
5. Kalenkov G.S., Kalenkov S.G., Shtan'ko A.E. *Quantum Electron*., **45** (4), 333 (2015) [*Kvantovaya Elektron*., **45** (4), 333 (2015)].
6. Kalenkov G.S., Kalenkov S.G., Shtan'ko A.E. *Izmerit. Tekhn*., (11), 21 (2012).
7. Shevkunov I., Katkovnik V., Claus D., Pedrini G., Petrov N.V., Egiazarian K. *Opt. Laser Eng*., **127**, 105973 (2020).
8. Shevkunov I., Katkovnik V., Claus D., Pedrini G., Petrov N.V., Egiazarian K. *Sensors*, **19**, 5188 (2019).
9. Pariente G., Gallet V., Borot A., Gobert O., Quere F. *Nat. Photonics*, **10**, 547 (2016).
10. Borot A., Quere F. *Opt. Express*, **26**, 26444 (2018).
11. Akturk S., Gu X., Bowlan P., Trebino R. *J. Opt.*, **12**, 093001 (2010).
12. Petrov N.V., Kulya M.S., Tsypkin A.N., Bespalov V.G., Gorodetsky A. *IEEE Trans. Terahertz Sci. Technol*., **6**, 464 (2016).
13. Kulya M.S., Semenova V.A., Bespalov V.G., Petrov N.V. *Sci. Rep*., **8**, 1 (2018).
14. Kulya M., Petrov N.V., Katkovnik V., Egiazarian K. *Appl. Opt*., **58**, G61 (2019).
15. Kulya M., Petrov N.V., Tsypkin A., Egiazarian K., Katkovnik V. *Opt. Express*, **27**, 18456 (2019).
16. Chizhov P.A. et al. *Quantum Electron*., **45** (5), 434 (2015) [*Kvantovaya Elektron*., **45** (5), 434 (2015)].
17. Gallot G., Grischkowsky D. *J. Opt. Soc. Am. B*, **16** (8), 1204 (1999).
18. Ushakov A. et al. *J. Opt. Soc. Am. B*, **35** (5), 1159 (2018).